BIOCHEMISTRY
including biophysical chemistry & molecular biology

Article

pubs.acs.org/biochemistry

Membrane Docking of the Synaptotagmin 7 C2A Domain: Computation Reveals Interplay between Electrostatic and Hydrophobic Contributions

Nara Lee Chon,[†] J. Ryan Osterberg,[†] Jack Henderson,[†] Hanif M. Khan,[‡,§] Nathalie Reuter,[‡,§] Jefferson D. Knight,[*,†] and Hai Lin[*,†]

[†]Department of Chemistry, University of Colorado Denver, Denver, Colorado 80217-3364, United States

[‡]Department of Molecular Biology, University of Bergen, 5008 Bergen, Norway

[§]Computational Biology Unit, Department of Informatics, University of Bergen, 5008 Bergen, Norway

Supporting Information

ABSTRACT: The C2A domain of synaptotagmin 7 (Syt7) is a Ca^{2+} and membrane binding module that docks and inserts into cellular membranes in response to elevated intracellular Ca^{2+} concentrations. Like other C2 domains, Syt7 C2A binds Ca^{2+} and membranes primarily through three loop regions; however, it docks at Ca^{2+} concentrations much lower than those required for other Syt C2A domains. To probe structural components of its unusually strong membrane docking, we conducted atomistic molecular dynamics simulations of Syt7 C2A under three conditions: in aqueous solution, in the proximity of a lipid bilayer membrane, and embedded in the membrane. The simulations of membrane-free protein indicate that Syt7 C2A likely binds three Ca^{2+} ions in aqueous solution, consistent with prior experimental reports. Upon membrane docking, the outermost Ca^{2+} ion interacts directly with lipid headgroups, while the other two Ca^{2+} ions remain chelated by the protein. The membrane-bound domain was observed to exhibit large-amplitude swinging motions relative to the membrane surface, varying by up to 70° between a more parallel and a more perpendicular orientation, both during and after insertion of the Ca^{2+} binding loops into the membrane. The computed orientation of the membrane-bound protein correlates well with experimental electron paramagnetic resonance measurements presented in the preceding paper (DOI: 10.1021/acs.biochem.5b00421). In particular, the strictly conserved residue Phe229 inserted stably ~4 Å below the average depth of lipid phosphate groups, providing critical hydrophobic interactions anchoring the domain in the membrane. Overall, the position and orientation of Syt7 C2A with respect to the membrane are consistent with experiments.

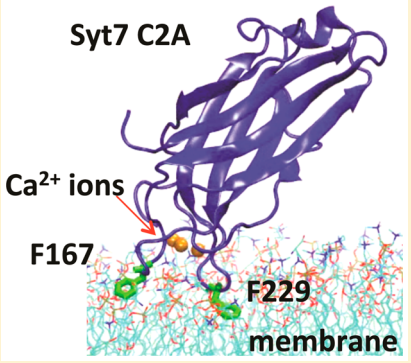

The synaptotagmin (Syt) family of proteins encompasses 17 human isoforms, including eight that are generally characterized as key Ca^{2+} sensors for membrane fusion during exocytosis.[1,2] Some well-documented actions of Syt isoforms include Syt1 regulation of neurotransmitter secretion and Syt7 dependence of insulin secretion in pancreatic β cells.[1,3,4] Syt binds Ca^{2+} and membranes through its two C2 domains, denoted C2A and C2B. C2 domains are a ubiquitous membrane binding motif and dock to lipid membranes primarily through their three Ca^{2+} binding loops [termed CBL1−CBL3 (see Figure S1 of the Supporting Information)].[5,6] Coordination of Ca^{2+} ions in the CBLs typically alters the electrostatic surface profile of a C2 domain, allowing its insertion into a target (in many cases anionic) lipid bilayer.

C2 domains exhibit varying degrees of electrostatic and hydrophobic interactions with their target membranes.[7−10] In particular, each isoform of Syt has evolved a precise function suited to its physiological context. For example, the C2 domains of Syt1 require high Ca^{2+} concentrations for activation and dock to membranes via primarily electrostatic interactions with fast kinetics of binding and release on time scales necessary for neurotransmitter secretion.[11−13] In contrast, previous studies have shown Syt7 C2A and C2AB to have kinetics much slower than those of their counterparts in Syt1.[1,10] Our recent measurements indicate that the membrane docking of Syt7 C2A includes a contribution from the hydrophobic effect much stronger than that of Syt1 C2A, even though the two closely related protein domains are very similar in structure.[10] This surprising finding leads us to hypothesize that Syt7 C2A is likely more deeply embedded in the membrane, a hypothesis that is tested by simulation and experiment in this paper and the preceding paper (DOI: 10.1021/acs.biochem.5b00421), respectively.

In the preceding paper, we use EPR spectroscopy to measure the membrane docking geometry of Syt7 C2A to directly compare it with a previously developed docking model of Syt1

Received: April 19, 2015
Revised: September 2, 2015
Published: September 2, 2015

DOI: 10.1021/acs.biochem.5b00422
Biochemistry 2015, 54, 5696−5711

C2A.[14] A comparison of the docking models finds that like Syt1 C2A, Syt7 C2A binds membranes primarily through its CBL3 and secondarily through its CBL1. CBL1 of Syt7 C2A, however, appears to penetrate deeper in comparison to Syt1, which may suggest a greater role for this binding loop in Syt7 C2A. However, the uncertainty in our EPR model is such that we cannot rule out the possibility of Syt1 C2A and Syt7 C2A binding at similar depths.

Here, we use molecular dynamics simulations with human Syt1 and Syt7 C2A domains to address the outstanding questions from the experimental study mentioned above, as well as to shed light on energetic factors underlying membrane binding and insertion by Syt7 C2A. In particular, we aim to gain insights into the following problems. (1) How many Ca^{2+} ions are most likely bound to Syt7 C2A? Experiments[15] have shown that, although Syt7 C2A can also bind three Ca^{2+} ions, the affinity for the third Ca^{2+} is much lower than those for the first two Ca^{2+} ions. Moreover, detailed structural information [from nuclear magnetic resonance (NMR) spectroscopy] is available only for the Ca^{2+}-free state of this domain.[16] Given that binding of Ca^{2+} ions is necessary for Syt7 C2A membrane docking, it is important to determine the most likely stoichiometry of binding of Ca^{2+} to Syt7 C2A. (2) What roles do the Ca^{2+} ions and the CBLs play in the process of Syt7 C2A approaching and associating with the membrane? Most experiments report on only equilibrium states of Syt7 C2A before and after membrane docking. A qualitative picture of the dynamic nature of the docking interaction is informative, particularly regarding how the Ca^{2+} ions and CBLs participate in transitions between the solution and membrane-docked states. (3) What kinds of equilibrium structures does Syt7 C2A adopt after docking into a membrane? Here we have conducted simulations without input from the experimental data reported in the preceding paper (DOI: 10.1021/acs.biochem.5b00421), i.e., membrane insertion depths and orientations. This approach stands in contrast to prior collaborative EPR/simulation studies and allows us to make predictions to be compared with the experimental measurements.

To facilitate comparisons with the EPR measurements, the simulations were designed to replicate the experimental conditions wherever possible, including equivalent lipid composition and solution ionic strength. Repeat simulations were performed from multiple initial starting geometries of the Syt7 C2A domain relative to the lipid bilayer. Importantly, all simulations were conducted naïve to the final experimentally determined Syt7 C2A docking geometry. Overall, the simulations provide a detailed picture of the structure, dynamics, and energetics of Syt7 C2A membrane docking that is consistent with and complementary to the experimental results.

COMPUTATIONS

While our simulations of membrane docking focus on the Syt7 C2A domain, we also conducted certain calculations in the absence of lipid on the Syt1 C2A domain for the purpose of comparison. A brief description of the models and computational methods is given below, with additional details provided in section 1 and Tables S1−S3 of the Supporting Information.

Stand-alone Membrane. A phospholipid bilayer model was built by mixing 1-palmitoyl-2-oleoyl-*sn*-glycero-3-phosphocholine (POPC) and 1-palmitoyl-2-oleoyl-*sn*-glycero-3-phospho-L-serine (POPS) at a molar ratio of 3:1 (Figure 1). The model was constructed employing Membrane Builder in

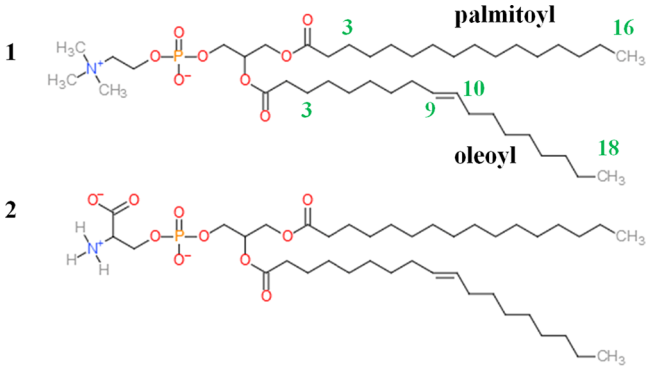

Figure 1. Structures of 1-palmitoyl-2-oleoyl-*sn*-glycero-3-phosphocholine (POPC, **1**) and 1-palmitoyl-2-oleoyl-*sn*-glycero-3-phospho-L-serine (POPS, **2**).

CHARMM-GUI[17] and is described by the Charmm36[18] force fields and TIP3P[19] water model. It contained 192 POPC lipids, 64 POPS lipids, 64 Na^+ counterions, and 9219 water molecules (Table S1 of the Supporting Information). Using NAMD,[20] the model was equilibrated at 310 K and 1 bar for 160 ns under the *NpT* ensemble with a periodic boundary.

Stand-alone Proteins. Structural manipulations were performed using VMD,[24] and the minimizations and MD simulations were performed using NAMD,[20] with Charmm22[21−23] force fields. We began with the Syt1 C2A model, for which the Ca^{2+}-bound structure [Protein Data Bank (PDB) entry 1BYN[25]] is available. In this structure, the first Ca^{2+} ion is coordinated by the side chains of D172, D178, D230, and D232 and the backbone oxygen of residue F231; the second Ca^{2+} ion by the side chains of D172, D230, D232, and D238 and the backbone oxygen of residue L171; and the third Ca^{2+} ion by the side chains of D232, S235, and D238 and the backbone oxygen of residue K236. After the missing hydrogen atoms were added, the protein was solvated in a box of pre-equilibrated TIP3P[19] water molecules. The system was neutralized by substituting randomly selected water molecules with Cl^- ions. The protein−solvent complex was then minimized for 1000 steps, followed by a slow heating from 0 to 298 K over 440 ps and a final equilibration at 298 K and 1 bar for 200 ns.

The solvated Syt7 C2A domain was prepared using the same protocol. However, for Syt7 C2A, only the Ca^{2+}-free experimental structure (PDB entry 2D8K[16]) is available. This complicates the procedure as Syt7 C2A can also bind three Ca^{2+} ions, with a K_d of ∼200 μM for each of the first two Ca^{2+} ions and a weaker affinity for the third Ca^{2+} ion.[15] Therefore, we conducted two different simulations for the solvated Syt7 C2A domain, in which we added two and three Ca^{2+} ions to the Ca^{2+}-free Syt7 C2A structure (section 1.2 of the Supporting Information). The compositions of the models are given in Table S1 of the Supporting Information.

Figure 2A provides an overview of the Ca^{2+} binding site in Syt7 C2A, and Figure 2B−D shows a detailed view of the bound Ca^{2+} ions within the models of the Syt1 and Syt7 C2A domains after minimization. MD simulations of the stand-alone C2A domains were initiated from these geometries, and the data (details in Results) suggest that all model systems are stable in the simulations. This implies that the Ca^{2+}-free experimental structure of Syt7 C2A is reasonably accurate for building the Ca^{2+}-bound systems, allowing fast equilibrations in solution. As described in the Results, Syt7 C2A appeared to be

DOI: 10.1021/acs.biochem.5b00422
Biochemistry 2015, 54, 5696−5711

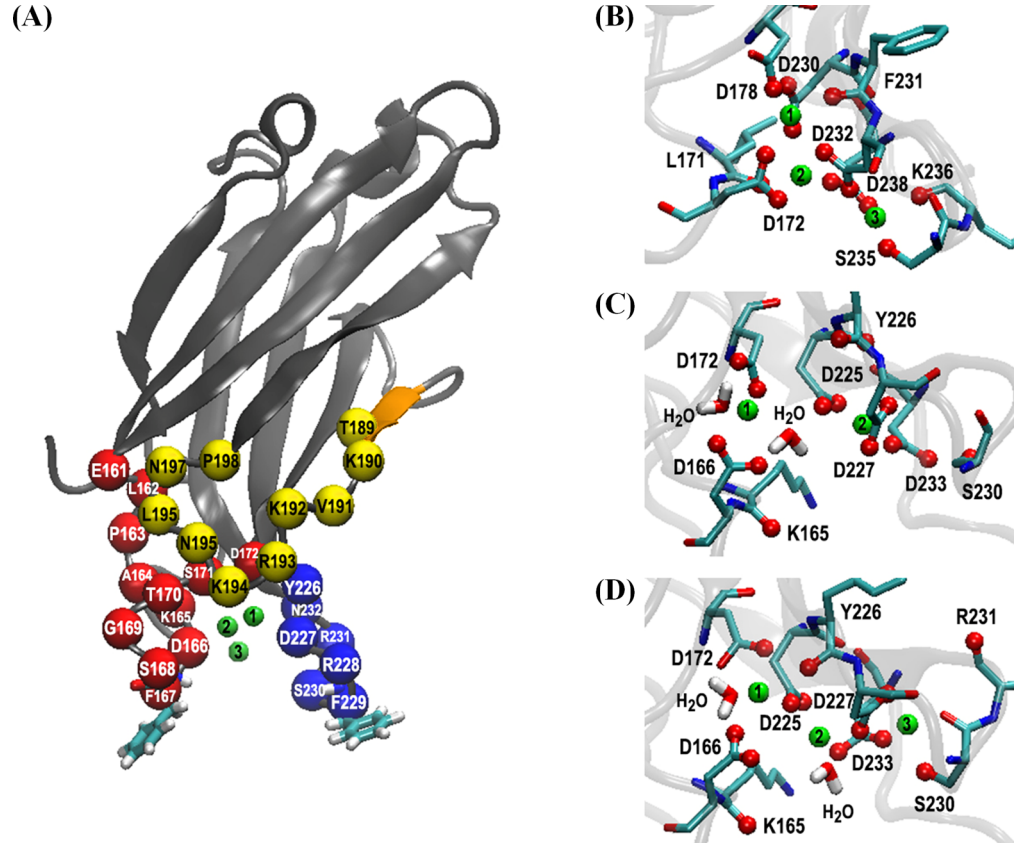

Figure 2. Ca^{2+} coordination by Syt1 and Syt7 C2A domains. (A) Overview of the Ca^{2+} binding region of Syt7 C2A. The three Ca^{2+} ions are represented by small green spheres with labels 1−3. The protein is colored gray (β4 in orange), with the residues belonging to Ca^{2+} binding loops indicated by red, yellow, and blue spheres for CBL1−CBL3, respectively. The side chains of the two critical phenylalanine residues, F167 and F229, are represented as licorice (white, H; cyan, C). (B−D) Detailed views of Ca^{2+} ions after minimizations in the binding sites of the models of (B) Syt1 C2A with three Ca^{2+} ions, (C) Syt7 C2A with two Ca^{2+} ions, and (D) Syt7 C2A with three Ca^{2+} ions. Ca^{2+} ions are green spheres with surrounding residues shown as licorice (cyan, C; blue, N; red, O), and the O atoms coordinating the Ca^{2+} ions are shown as red spheres. For the sake of clarity, protein H atoms are not shown.

somewhat more stable in the presence of three Ca^{2+} ions than in the presence of two Ca^{2+} ions. Binding to three Ca^{2+} ions was therefore deemed the more likely stoichiometry, so the equilibrated Syt7 C2A domain with three Ca^{2+} ions was used for construction of the protein−membrane complex models. Snapshots of the stand-alone Syt7 C2A and Syt1 C2A simulations bound to three Ca^{2+} ions (at 6, 8, and 10 ns) also served as the starting structures for EPR docking geometry modeling as described in the preceding paper (DOI: 10.1021/acs.biochem.5b00421).

In addition to MD simulations, we also conducted Poisson−Boltzmann calculations of the surface electrostatic potentials using the Adaptive Poisson−Boltzmann Solver[26] for the NMR structures of Syt1 C2A and Syt7 C2A. Calculations were performed for Ca^{2+}-bound and Ca^{2+}-free forms (section 1.3 of the Supporting Information).

Syt7 C2A Protein−Membrane Complexes. To prepare Syt7 C2A−membrane complexes for simulation, structures were manipulated using CHARMM[21] and VMD, and minimization and MD simulations were performed using NAMD.[20] Two types of model systems were employed for the Syt7 C2A−membrane complex, and two simulations were conducted for each type of model system, for a total of four 500-ns simulations. First, we simulated two "pre-insertion" complexes, in which the Ca^{2+}-bound Syt7 C2A domain was initially placed above the membrane in two different orientations: (i) a "lying-down" model in which the long axis of the domain was tilted by 23° toward the membrane surface (Figure 3A) and (ii) a "standing-up" model in which the long axis of the domain was more perpendicular (tilt angle of 36°) to the membrane surface (Figure 3B). The definition of tilt angle for the protein with respect to the membrane plane is given in Figure 4. In the lying-down model, the Syt7 C2A tilt angle is similar to the previously reported Syt1 C2A experimental docking geometry,[14] while in the standing-up model, Syt7 C2A was oriented such that loops CBL1 and CBL3 were similar distances from the membrane. The α-carbon atom (C_α) of F229 of CBL3 was in the aqueous phase, above the average phosphate plane of the membrane by 6.9 and 4.2 Å in the lying-down and standing-up models, respectively (Figure 3D). After solvation, both models were minimized for 18000 steps using NAMD with gradually relaxed harmonic restraints (Table S2 of the Supporting Information). MD simulations were conducted under the *NpT* ensemble at 298 K and 1 bar, first for 800 ps with a frozen protein backbone and restrained Ca^{2+} ion solvation shells [harmonic restraints on the distances between the Ca^{2+} ions and their coordinating oxygen atoms (see Table S3 of the Supporting Information)], then for 2 ns with only the restrained Ca^{2+} ion solvation shells, and finally for 500 ns without any constraint or restraint.

Second, we simulated two "embedded" complexes, in which the C2A domains were modeled in a membrane-inserted state

DOI: 10.1021/acs.biochem.5b00422
Biochemistry 2015, 54, 5696−5711

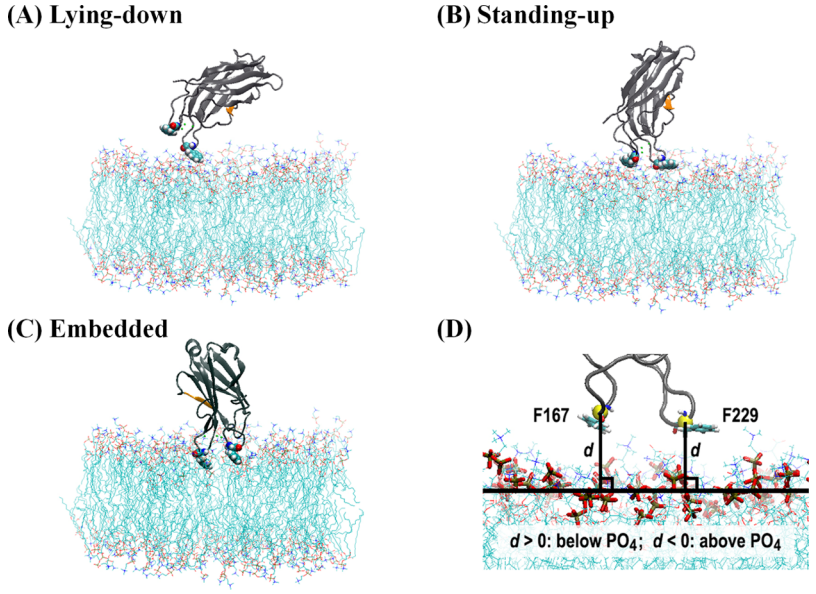

Figure 3. Initial models used for simulation of protein−membrane complexes. In the preinsertion models, the protein was placed above the membrane, and either (A) angled toward the membrane in the lying-down model or (B) approximately perpendicular to the membrane plane in the standing-up model (initial penetration depths of F229 of CBL3, −6.9 Å for the lying-down model and −4.2 Å for the standing-up model). (C) In the embedded models, CBL1 and CBL3 were inserted into the membrane by 1.8 Å and the protein remained approximately perpendicular to the membrane plane throughout the simulation. The protein is represented by a cartoon (β4 in orange); residues F167 and F229 are represented by van der Waals spheres and the lipids by lines. (D) Distance d between a residue and the membrane measured from the C_α position (yellow sphere) to the average phosphate plane of the membrane (black horizontal line). Lipids are shown as lines except phosphate atoms as licorice. Color code: red, O; cyan, C; blue, N; tan, P; white, H.

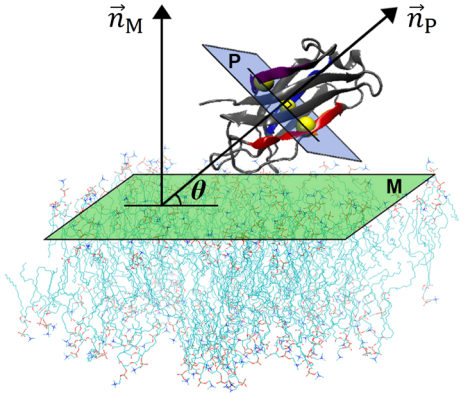

Figure 4. Definition of the tilt angle of the Syt7 C2A domain with respect to the average membrane phosphate plane M (green shaded area), which is parallel to the x−y plane. A cross section of the protein (plane P, the blue shaded area) is determined by the centers of mass (yellow spheres) of three outermost β-strands (β5, red; β6, blue; β8, purple). Tilt angle θ is calculated as the angle between $\vec{n}_p$ (the normal vector of plane P) and membrane plane M.

(Figure 3C). Two models were created, each with the protein inserted into the membrane and three overlapping POPC lipids deleted. In both embedded models, the C_α atom for F167 of CBL1 was positioned above the average phosphate plane by 1.4 Å while the C_α atom for F229 of CBL3 was below by 1.8 Å on average. However, both side chain phenyl rings were embedded in the membrane (Table S4 of the Supporting Information). The initial tilt angles were 48° and 35° for the first and second embedded models, respectively. The starting protein conformations in the two embedded models were similar except for one noticeable difference: the side chain of K184 was near the membrane in the first model but oriented away from the membrane in the second model, as illustrated in Figure S2 of the Supporting Information. Solvation, minimizations, and MD simulations were performed for the embedded models as described for the preinsertion models. On the basis of the volume of the primary cell and number of ions, the effective concentration of Na^+ in the solution was 120−140 mM in all models, closely similar to the monovalent cation (K^+) concentration of 150 mM used in the experimental study. To test whether C2A membrane association depends on monovalent cation identity, we additionally conducted a simulation of the standing-up protein−membrane complex in K^+ rather than Na^+. The results are shown in the Supporting Information (Table S8 and Figure S12) and are overall consistent with those from the Na^+ simulations described here, suggesting that specific ion effects are minimal. All models are also described further in the Supporting Information (section 1 and Table S1).

RESULTS

Simulation of the 3:1 PC/PS Membrane. First, simulations were conducted with the membrane alone with water and Na^+ ions. The area per lipid (APL) is plotted in Figure S3A of the Supporting Information as a function of simulation time for the 3:1 POPC/POPS lipid bilayer. The value of APL dropped quickly within the first 8 ns but became reasonably stable after simulation for 20 ns. Averaging over the fully equilibrated final 120 ns (from 40 to 160 ns) yields an average APL of 62.6 ± 0.9 $Å^2$, which is very close to the value of 62.9 $Å^2$ predicted from the literature values of pure POPC and pure POPS membranes (Table 1). The membrane order parameters for individual carbon positions obtained from our simulations are displayed in Figure S3B. As expected, order parameters for the palmitoyl chain generally fall between those for pure POPC[27] and pure POPS.[28] For the oleoyl chain, there

DOI: 10.1021/acs.biochem.5b00422
Biochemistry 2015, 54, 5696−5711

Table 1. Comparisons of Average Values of Area Per Lipid (APL) of Simulated Membranes

APL (Å^2)	pure POPC	pure POPS	POPC/POPS (3:1)
experiment	64.3 ± 1.3[a]	N/A	N/A
simulation	65.5 ± 1.1[b]	55 ± 1.0[c]	62.9 ± 0.9,[d] 62.6 ± 0.9[e]

[a]From ref 58. [b]From ref 59. [c]From ref 60. [d]Estimated as $0.75APL_{POPC}$ + $0.25APL_{POPS}$ based on the values in refs 59 and 60. [e]This work, average over the last 120 ns of the 160 ns simulation.

are no prior data for pure POPS and limited data for pure POPC[27] for comparison; our results agree reasonably well with the available POPC data. Overall, the APL and order parameters obtained from our simulations indicate that the membrane model is reasonably accurate and was well equilibrated after 40 ns.

Simulation of the Syt7 C2A Domain Alone and Bound to Ca^{2+}. The protein models of Syt1 and Syt7 C2A domains were based on the structures resolved by multidimensional NMR spectroscopy.[16,25] Structures of Syt1 C2A both Ca^{2+}-free[29] and bound to three Ca^{2+} ions[25] are available, while the single available structure of Syt7 C2A is Ca^{2+}-free.[16] Ca^{2+}-sensitive C2 domains generally bind between one and four Ca^{2+} ions, and Syt7 C2A has been shown to bind up to three Ca^{2+} ions (two with K_d values of ∼200 μM and one more weakly).[5,15,30−32] Therefore, we generated starting geometries of the Syt7 C2A domain structure bound to two or three Ca^{2+} ions as described in Computations, both to probe its Ca^{2+} binding stoichiometry and to prepare for simulations of protein−membrane docking. Although the first and second Ca^{2+} ions were originally placed at the same locations in the two-Ca^{2+} and three-Ca^{2+} models, minimizations led to different coordination structures of the first and second Ca^{2+} ions in those two models. The locations of the Ca^{2+} ions after minimizations in the three-Ca^{2+} model were similar to those in the Ca^{2+}-bound Syt1 C2A experimental structure.[25] The first Ca^{2+} ion was coordinated by the side chains of D166, D172, D225, and D227, the backbone oxygen of residue Y226, and one water molecule; the second Ca^{2+} ion by the side chains of D166, D225, D227, and D233, the backbone oxygen of residue K165, and one water molecule; and the third Ca^{2+} ion by the side chains of D227, S230, and D233 and the backbone oxygen of residue R231. In the two-Ca^{2+} model, however, the second Ca^{2+} ion moved toward CBL3, and the side chains that coordinated the Ca^{2+} ions took somewhat different orientations. As a result, the first Ca^{2+} ion was coordinated by the side chains of D166 and D172, the backbone oxygens of residues K165 and Y226, and two water molecules and the second Ca^{2+} ion by the side chains of D225, D227, S230, and D233.

Using the starting geometries described above, trajectories of 200 ns were generated for each of the three proteins (Syt1 C2A with three Ca^{2+} ions and Syt7 C2A with two and three Ca^{2+} ions). The protein conformations were overall quite stable, as can be seen from the consistently small root-mean-square deviation (rmsd) (with respect to the starting geometry) of the protein backbone heavy atoms (N, C, O, and C_α) during the simulation in Figure S4A. The rapid equilibration confirms that the initial models built from experimental structures are reasonably accurate. The average rmsd of the protein backbone was 1.1 Å for Syt1 C2A, substantially smaller than the value of 2.6 Å for Syt7 C2A with two Ca^{2+} ions and somewhat smaller than the value of 1.8 Å for Syt7 C2A with three Ca^{2+} ions (Table 2). Although all of these rmsd values are quite small, it is perhaps not surprising that those of Syt1 C2A were smallest; its starting geometry was based on a Ca^{2+}-bound NMR structure, whereas the Syt7 C2A starting geometries were built by adding Ca^{2+} ions to a Ca^{2+}-free structure.

The coordination shells for the Ca^{2+} ions were largely maintained during the entire simulations of Syt1 and Syt7 C2A bound to three Ca^{2+} ions. However, both coordination shells changed during the simulation of Syt7 C2A with two Ca^{2+} ions. The variations of the position of the Ca^{2+} ions and CBLs with respect to their initial position are smaller in the simulations with three Ca^{2+} ions than in the simulation with two Ca^{2+} ions. Strikingly, the rmsd values for the first Ca^{2+} (1.0 Å) and second Ca^{2+} (0.5 Å) ions in the three-Ca^{2+} Syt7 C2A simulation were similar to those (both 0.5 Å) in Syt1 C2A with three Ca^{2+} ions but are considerably smaller than those (3.2 and 1.8 Å) in the two-Ca^{2+} Syt7 C2A simulation. The differences in rmsd between the three- and two-Ca^{2+} models, although moderate, suggest that the binding of the third Ca^{2+} ion stabilizes the other two bound Ca^{2+} ions and the backbone of the CBLs.

Coordination of three Ca^{2+} ions is similar between Syt1 and Syt7 C2A, as illustrated by the distances between the Ca^{2+} ions and each coordinating oxygen atom from the protein (Figure 5). Plots of these distances as a function of simulation time indicate a subtle conformational change in Syt7 C2A around 3

Table 2. Root-Mean-Square Deviations (rmsd) in Angstroms, Averaged over the Trajectories for Selected Atoms in the Simulations of Stand-alone Proteins and Protein−Membrane Complexes[a]

		backbone[b]	first Ca^{2+}	second Ca^{2+}	third Ca^{2+}
Stand-alone Proteins					
Syt1 3-Ca^{2+}	200 ns[c]	1.1 ± 0.1 (1.5)	0.5 ± 0.2 (1.1)	0.5 ± 0.2 (1.3)	4.1 ± 0.3 (6.0)
Syt7 2-Ca^{2+}	200 ns[c]	2.6 ± 0.2 (3.5)	3.2 ± 0.7 (5.1)	1.8 ± 0.5 (3.6)	N/A
Syt7 3-Ca^{2+}	200 ns[c]	1.8 ± 0.1 (2.4)	1.0 ± 0.2 (1.8)	0.5 ± 0.2 (1.2)	2.4 ± 0.4 (4.0)
Protein−Membrane Complexes					
preinsertion					
lying-down	500 ns[d]	1.5 ± 0.1 (2.2)	0.4 ± 0.2 (1.2)	0.4 ± 0.2 (1.4)	2.0 ± 0.4 (4.7)
standing-up	500 ns[d]	1.4 ± 0.1 (2.0)	0.4 ± 0.2 (1.0)	0.4 ± 0.2 (1.1)	2.4 ± 0.3 (3.8)
embedded					
first	500 ns[d]	1.1 ± 0.1 (1.6)	0.5 ± 0.2 (1.4)	0.5 ± 0.2 (1.3)	1.1 ± 0.5 (2.8)
second	500 ns[d]	1.2 ± 0.2 (1.9)	0.5 ± 0.2 (1.3)	0.7 ± 0.2 (1.6)	1.1 ± 0.3 (2.3)

[a]The maximum rmsd values are given in parentheses. Mean ± the standard deviation with respect to the initial structure. [b]Protein backbone heavy atoms N, C, O, and C_α. [c]Calculated using the last 80 ns of trajectories from 200 ns stand-alone protein simulations. [d]Calculated using the last 400 ns of trajectories from 500 ns protein−membrane simulations.

DOI: 10.1021/acs.biochem.5b00422
Biochemistry 2015, 54, 5696−5711

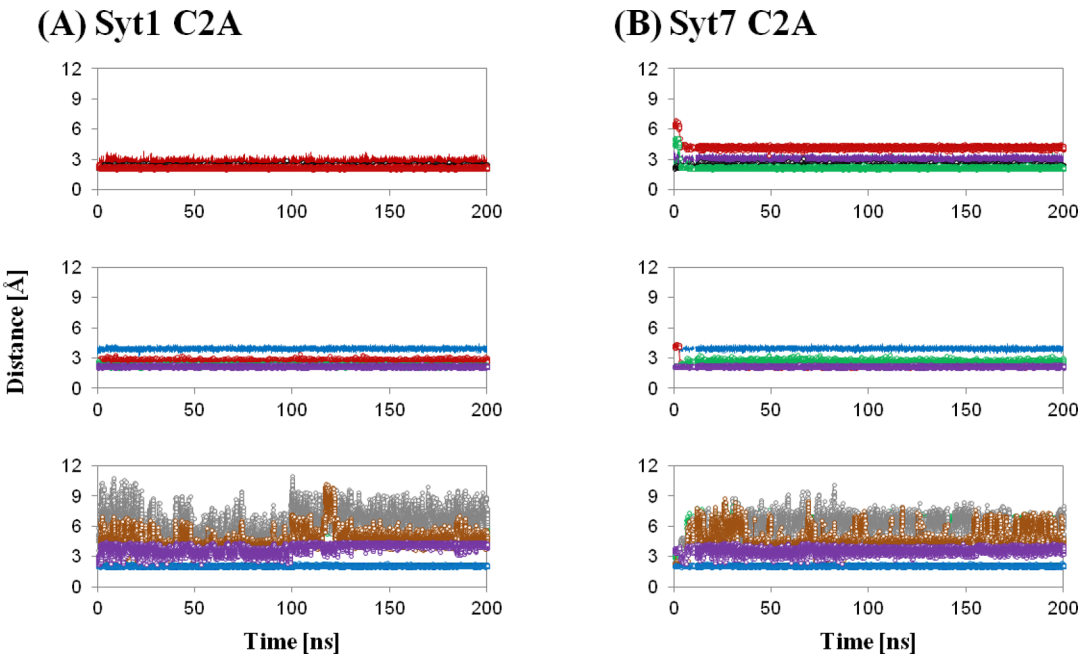

Figure 5. Distances between each Ca^{2+} ion and its coordinating protein oxygen atoms, as a function of time in the 200 ns simulations of stand-alone (A) Syt1 and (B) Syt7 C2A with three Ca^{2+} ions. In each column, the top, middle, and bottom panels are for the first, second, and third Ca^{2+} ions, respectively. Color code in panel A: L171 O, black; D172 OD1, red; D172 OD2, green; D178 OD2, gray; D230 OD1, blue; D230 OD2, purple; F231 O, black with markers; D232 OD1, red with markers; D232 OD2, green with markers; S235 OG, gray with markers; K236 O, brown with markers; D238 OD1, blue with markers; and D238 OD2, purple with markers. Color code in panel B: K165 O, black; D166 OD1, red; D166 OD2, green; D172 OD2, gray; D225 OD1, blue; D225 OD2, purple; Y226 O, black with markers; D227 OD1, red with markers; D227 OD2, green with markers; S230 OG, gray with markers; R231 O, brown with markers; D233 OD1, blue with markers; and D233 OD2, purple with markers.

ns, which brought the D227 side chain nearer the first and second Ca^{2+} ions and weakened the coordination between the third Ca^{2+} ion and the D227 and S230 side chains. The conformational change stabilized the first and second Ca^{2+} ions and destabilized the third Ca^{2+} ion to some extent. The Ca^{2+} coordination in Syt7 C2A became more similar to that in Syt1 C2A after the conformational change. Further analysis is provided in Table 3, in which the average distances between the Ca^{2+} ions and their coordinating oxygen atoms from the CBLs are calculated for the final 80 ns of the simulations of Syt1 and Syt7 C2A with three Ca^{2+} ions. The results indicate that, in both Syt1 and Syt7 C2A, the first and second Ca^{2+} ions are tightly held by the loops, whereas the third Ca^{2+} ion binds less tightly, primarily through interactions with an aspartate side chain (D238 in Syt1 and D233 in Syt7) and secondarily by an oxygen in the backbone (K236 in Syt1 and R231 in Syt7). The resemblance between the Syt1 and Syt7 results strongly suggests that Syt7 C2A binds three Ca^{2+} ions in a manner similar to that of Syt1 C2A, in agreement with previous NMR measurements;[15] therefore, subsequent calculations were conducted using this state of the Syt7 C2A domain.

The electrostatic potentials of Syt1 and Syt7 C2A domains from Poisson−Boltzmann calculations are shown in Figure 6 and Figure S5. As expected, the two C2A domains have overall similar electrostatic potentials. For example, the Ca^{2+} binding sites in both C2A domains have negative potentials in the Ca^{2+}-free structures, because of the aspartate residues and the exposed backbone oxygen atoms in the Ca^{2+} binding loops (Figure 2). The binding of three Ca^{2+} ions renders the potentials of the membrane binding surfaces positive. Furthermore, in both C2A domains, the β4 strand and adjacent loops feature a cluster of lysine and arginine residues, giving rise to positive potentials in that region even in the absence of Ca^{2+}

Table 3. Means ± the Standard Deviation for the Distances (in angstroms) between Ca^{2+} Ions and Their Coordinating Oxygen Atoms from the Loops in the Ca^{2+} Binding Site, Averaged over the Final 80 ns of the Simulations of Syt1 and Syt7 C2A Domains[a]

	Syt1 3-Ca^{2+}			Syt7 3-Ca^{2+}		
ion	residue	atom	distance	residue	atom	distance
first Ca^{2+}	D172	OD1	2.6 ± 0.2	D166	OD1	2.2 ± 0.1
	D172	OD2	2.1 ± 0.1	D166	OD2	2.5 ± 0.2
	D178	OD2	2.1 ± 0.1	D172	OD2	2.1 ± 0.1
	D230	OD1	2.1 ± 0.1	D225	OD1	2.1 ± 0.1
	F231	O	2.3 ± 0.1	D225	OD2	3.1 ± 0.2
	D232	OD1	2.2 ± 0.1	Y226	O	2.3 ± 0.1
				D227	OD1	4.2 ± 0.1
				D227	OD2	2.2 ± 0.1
second Ca^{2+}	L171	O	2.3 ± 0.1	K165	O	2.3 ± 0.1
	D172	OD1	2.2 ± 0.1	D166	OD2	2.2 ± 0.1
	D230	OD1	3.9 ± 0.1	D225	OD1	3.9 ± 0.1
	D230	OD2	2.1 ± 0.1	D225	OD2	2.1 ± 0.1
	D232	OD1	2.5 ± 0.2	D227	OD1	2.2 ± 0.1
	D232	OD2	2.2 ± 0.1	D227	OD2	2.5 ± 0.1
	D238	OD2	2.1 ± 0.1	D233	OD2	2.1 ± 0.1
third Ca^{2+}	D232	OD2	6.0 ± 0.2	D227	OD2	6.6 ± 0.2
	S235	OG	6.9 ± 0.8	S230	OG	5.7 ± 0.9
	K236	O	4.8 ± 0.7	R231	O	4.9 ± 0.9
	D238	OD1	2.1 ± 0.1	D233	OD1	2.1 ± 0.1
	D238	OD2	4.2 ± 0.2	D233	OD2	3.7 ± 0.2

[a]Corresponding atoms in the two proteins are shown on the same line.

DOI: 10.1021/acs.biochem.5b00422
Biochemistry 2015, 54, 5696−5711

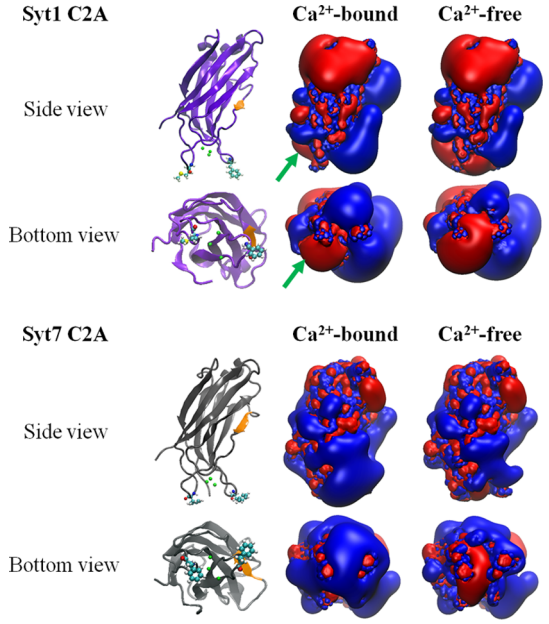

Figure 6. Electrostatic potential isosurfaces for the C2A domains of Syt1 (top) and Syt7 (bottom). In the left panel, the protein is shown as a cartoon with β4 colored orange, Ca^{2+} ions as green spheres, and the two hydrophobic residues at the tips of CBL1 and CBL3 (M173 and F234 in Syt1 C2A and F167 and F229 in Syt7 C2A) in ball-and-stick representation (N, blue; O, red; S, yellow; C, cyan; H, white). The middle and right panels display the potential maps computed with and without the three Ca^{2+} ions, respectively. Blue for positive (+1.5 mV equipotential contour) and red for negative (−1.5 mV equipotential contour). Note that a portion of the Ca^{2+} binding site in Syt1 C2A, but not Syt7 C2A, retains negative potential after Ca^{2+} binding (green arrows).

ions. The positive potentials of this region are enhanced somewhat in the Ca^{2+}-bound state. For the isolated C2A domains, the positive potentials offered by the β4 strand and adjacent loops may contribute to an electrostatic attraction between the protein and negatively charged lipids (e.g., POPS) in the membrane. However, the influence of the Ca^{2+} ions on the electrostatic potentials clearly confirms experimental results that show that the Ca^{2+} ions are critical to triggering C2A domain association with anionic membranes.[10,30,33]

Beyond the overall similarity, subtle differences exist between the electrostatic potentials of the Syt1 and Syt7 C2A domains. For example, the overall electrostatic potential of Syt1 C2A is more negative than that of Syt7 C2A. A portion of the Ca^{2+} binding site in Syt1 C2A retains negative potential after Ca^{2+} binding (green arrows in Figure 6), whereas the entire CBL region in Syt7 C2A becomes positive upon binding Ca^{2+} ions. This suggests that Syt7 C2A may have a greater number of Ca^{2+}-dependent electrostatic interactions with anionic membranes.

Simulation of Protein−Membrane Docking. The structures and orientations of membrane-bound C2 domains have been the subject of many previous studies.[14,34−42] One parameter frequently used to simplify characterization of docking geometry is the tilt angle between the protein and the membrane, although the definition of this tilt angle has varied among different studies.[41] Here, we use the tilt angle defined in Figure 4 as one parameter for characterizing four independent simulations of Syt7 C2A membrane docking (see Computations).

In the first two simulations, the Syt7 C2A domain was initially placed above the membrane in a preinsertion state (Figure 3), with its long axis either approximately perpendicular to the membrane (standing-up model) or tilted farther toward the membrane surface similar to the reported orientation of Syt1 C2A[14] (lying-down model). In both models, the C_α atom of F229 was placed in the aqueous medium above the lipid phosphate plane, by 6.9 Å for the lying-down model and 4.2 Å for the standing-up model. Figure 7 plots the tilt angle together with the penetration depths of (1) the protein center of mass, (2) F167, and (3) F229 over the simulation time. In both the lying-down and standing-up models, the protein center of mass moved rapidly toward the membrane, from approximately −30 to approximately −20 Å within the first 50 ns (~0.2 Å/ns), even though no artificial force was used to guide the protein toward the membrane. (Note that we have adopted the sign convention of EPR experimentalists, in which more positive values indicate deeper penetration into the membrane.) During the first 50 ns, F229 started making contact with lipid headgroups, and the protein began to insert into the membrane. F229 was largely inserted into the membrane by 100 ns, with the average C_α position 0.8 Å below the lipid phosphate plane in the lying-down model and 2.8 Å below in the standing-up model.

The proteins in the two preinsertion model simulations did not converge to the same orientation during the 500 ns simulations, and it is possible that neither insertion is complete over this time scale, as the depths for the protein center of mass continue to increase slowly (~0.01 Å/ns) in the standing-up model and negligibly in the lying-down model after the first 100 ns. During most of the simulation time, the C2A domain in the lying-down model remained nearly parallel to the membrane plane, whereas the standing-up model retained more perpendicular orientations. The average tilt angles over the final 400 ns of simulation are 13.5 ± 10.0° for the lying-down model and 37.1 ± 9.5° for the standing-up model (Table 4). The more parallel lying-down orientation is presumably less favorable for penetration than the more perpendicular standing-up orientation. Interestingly, both simulations produced large-amplitude swinging motions of the protein between a more parallel and a more perpendicular orientation. The swinging motion was observed both before and after insertion of CBL3 and CBL1 into the membrane. The trend was especially prominent for the standing-up model, whose tilt angle fluctuated from 30° to 60° and back five times over the 500-ns simulation.

The plots of penetration depth in Figure 7 show that F229 stayed at or below the membrane phosphate plane after insertion into the membrane at ~100 ns (blue traces). In contrast, F167 did not remain stably inserted in the membrane (red traces). In the lying-down simulation, F167 stayed above the phosphate plane during the entire 500 ns. In the standing-up simulation, its penetration depth fluctuated between 5 and −12 Å for the final 400 ns, although it penetrated as deeply as F229 for a brief period around the 385 ns mark.

One striking feature of these data is an approximate anticorrelation between the tilt angle and the F167 penetration depth (Figure 8 and also Figure S6 of the Supporting Information). We hypothesize that these motions of CBL1 (which contains F167) result from competition between two types of interactions: (1) electrostatic attraction of the positively charged residues in the β4 strand and adjacent loops for the negatively charged PS headgroups and (2) the

DOI: 10.1021/acs.biochem.5b00422
Biochemistry 2015, 54, 5696−5711

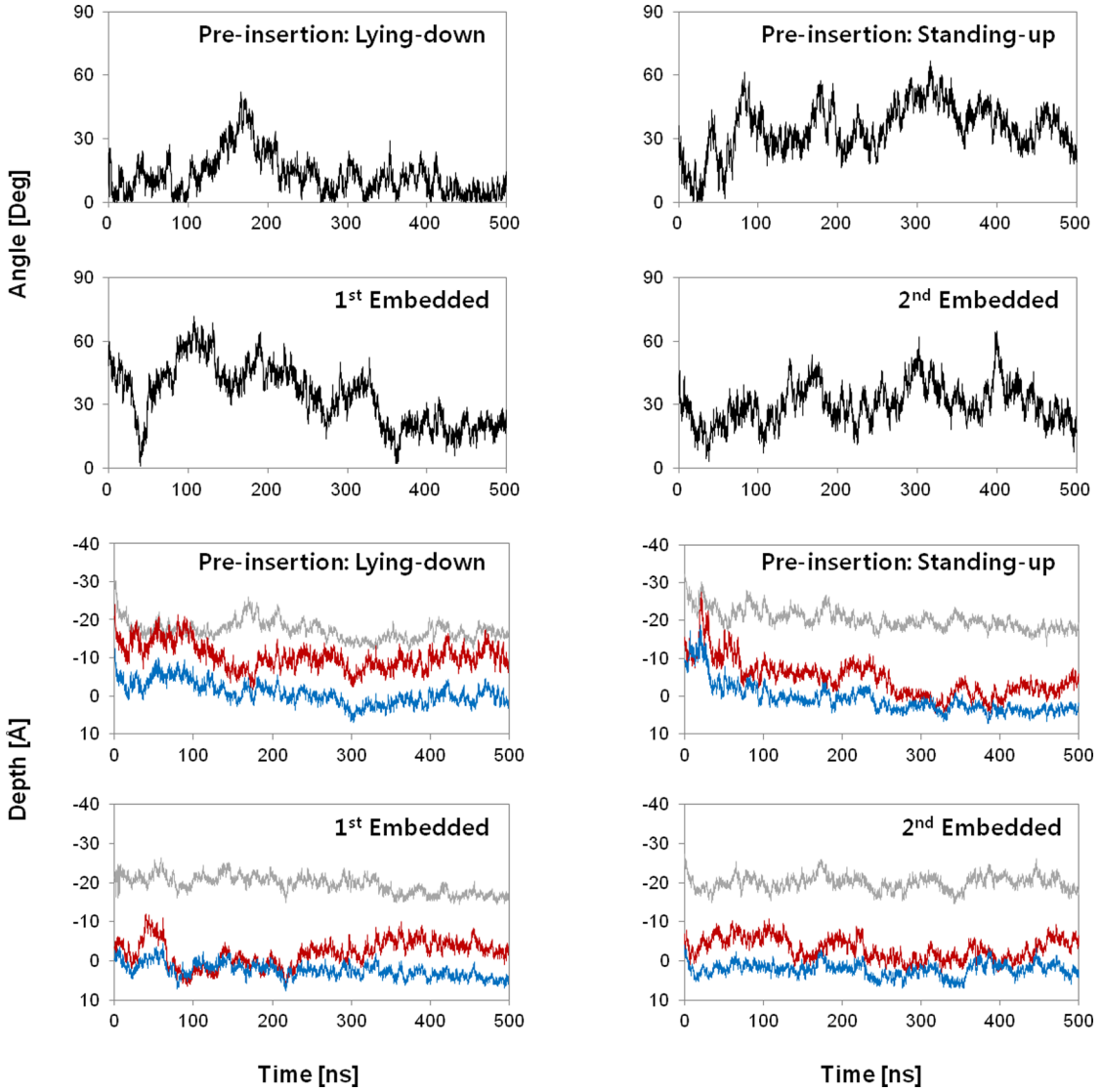

Figure 7. Tilt angles of the protein (black) and penetration depths of the protein center of mass (gray), F167 (red), and F229 (blue) for the indicated Syt7 C2A–membrane complex simulations over the simulation time.

Table 4. Statistics of Tilt Angle and Penetration Depth for F167 and F229, from the Simulations of Protein–Membrane Complexes[a]

			preinsertion		embedded	
			lying-down	standing-up	first model	second model
tilt angle (deg)	final 400 ns		13.5 ± 10.0	37.1 ± 9.5	32.8 ± 14.4	32.2 ± 9.1
depth (Å)	final 400 ns	F167	−9.8 ± 2.5	−3.1 ± 3.3	−2.0 ± 3.0	−2.6 ± 2.7
		F229	0.2 ± 2.2	2.2 ± 2.0	2.8 ± 1.6	2.4 ± 1.8
	final 100 ns	F167	−10.9 ± 2.1	−2.2 ± 1.7	−3.8 ± 1.5	−3.2 ± 2.6
		F229	0.0 ± 1.6	3.7 ± 0.9	4.1 ± 1.1	1.9 ± 1.4

[a]Mean ± the standard deviation. For the penetration depths, positive values indicate insertion deeper than the average phosphate plane while negative values indicate positions above the phosphate plane.

hydrophobic interactions between the phenyl ring of F167 and the lipid tails. For smaller values of the tilt angle, the positively charged residues were in the proximity of the lipid headgroups and F167 was not inserted. At larger tilt angles, the polybasic region was farther from the membrane and F167 was inserted. The competition and balance between the stabilization of F167 by the hydrophobic lipid tails and the electrostatic attraction of the positively charged residues by the lipid headgroups appeared to lead to a seesaw-like movement of the C2A domain with F229 at the fulcrum.

Embedded Protein–Membrane Complexes. Interestingly, the seesaw-like movements of the C2A domain were also observed for two simulations starting with the protein embedded in the membrane. Visual inspection of the trajectories reveals geometries similar to those after 200 ns in the preinsertion simulation with standing-up geometry. As

DOI: 10.1021/acs.biochem.5b00422
Biochemistry 2015, 54, 5696–5711

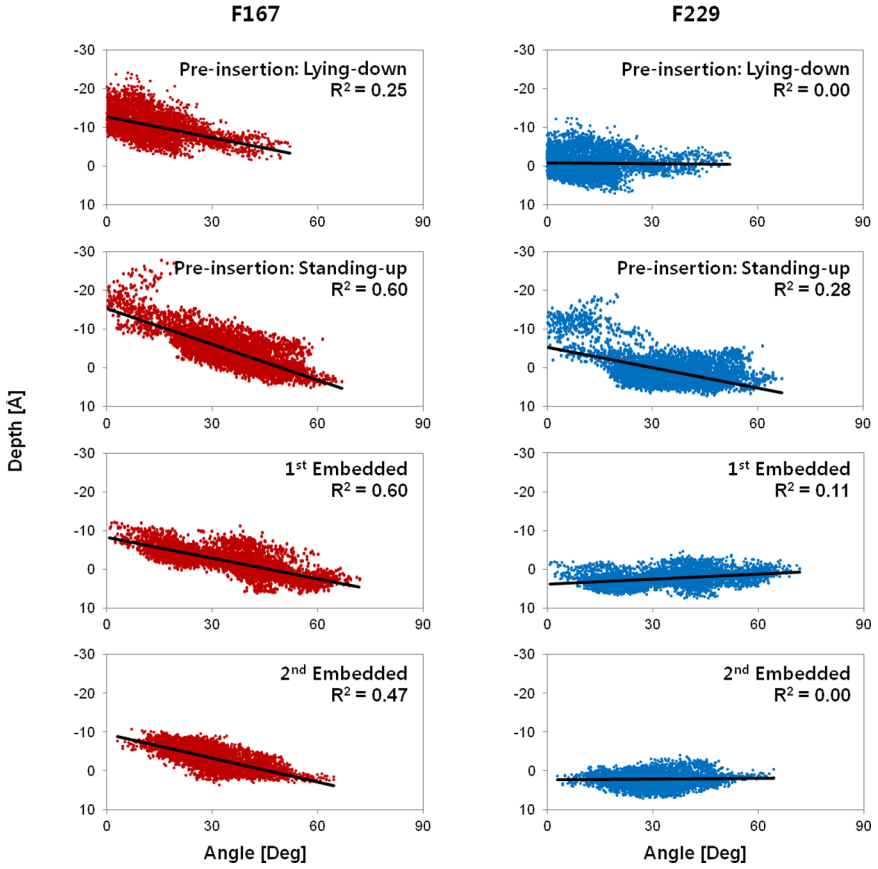

Figure 8. Penetration depths of F167 (red) and F229 (blue) vs the tilt angles of Syt7 C2A associated with the membrane, for each simulation of the protein−membrane complex.

illustrated in Figure 7, the tilt angles fluctuated notably with an amplitude of 10−30° and a frequency of roughly once per 100 ns, again showing an approximate anticorrelation with the penetration depth of F167 (see also Figure S6). Again, while F229 remained embedded below the phosphate plane, F167 sampled positions above and below the phosphate plane during the simulations. The average tilt angles of the protein and penetration depths of F167 and F229 are comparable to those for the preinsertion standing-up model (Table 4), suggesting the hydrophobic−electrostatic competition is also present in these simulations. In both embedded simulations and the standing-up simulation, the rates of penetration after 300 ns are either very slow (~0.01 Å/ns, first embedded model and standing-up model) or undetectable (second embedded model), suggesting that the protein reaches a stable or metastable penetration depth on the time scale of these simulations.

In both embedded models, CBL1 and CBL3 produce most of the contacts with the membrane. The total contacts between heavy atoms of the membrane and individual residues of the protein are plotted in Figure S7. Table 5 lists the 10 residues that have the most contacts with membrane lipid molecules in both simulations combined, and Table S5 provides a more complete list for each individual simulation. Overall, the contact numbers agree well between the first and second embedded simulations and indicate that residues from CBL1 and CBL3 have predominant interactions with the membrane. The only residue that showed substantial differences between the two embedded simulations is K184, which had more contacts with lipid headgroups in the first simulation. Visual inspection of the

Table 5. Residues with the Largest Numbers of Lipid Contacts, Averaged from the Two Embedded Simulations[a]

	no. of lipid contacts		depth (Å)	
residue	headgroups	acyl chains	last 400 ns[b]	last 100 ns[c]
F167	**46.9**	**19.9**	**−2.3 ± 2.0**	**−3.5 ± 1.5**
R231	**39.3**	**7.4**	**−1.8 ± 1.3**	**−1.1 ± 0.9**
G265	32.3	0.1	−4.9 ± 1.5	−4.5 ± 1.3
R228	**28.1**	**3.8**	**−0.3 ± 1.2**	**0.1 ± 0.9**
S230	**20.5**	**8.6**	**1.0 ± 1.2**	**1.3 ± 0.9**
S264	18.8	0	−6.5 ± 1.8	−6.8 ± 1.4
F229	**18.5**	**45.5**	**2.6 ± 1.2**	**3.0 ± 0.9**
S168	17.8	1.4	−3.5 ± 2.1	−5.0 ± 1.5
K194	14.8	0.1	−8.4 ± 1.6	−9.2 ± 1.2
D166	12.7	0	−4.5 ± 1.6	−5.3 ± 1.2

[a]Numbers of contacts are averaged over the last 400 ns of the simulations of the first and second embedded models. A cutoff of 5.0 Å was used in counting the heavy atom contacting pairs; i.e., if the distance between a heavy atom of the protein and a heavy atom of the lipids was less than 5.0 Å, this pair was counted. Entries for residues that average more than three interactions with acyl chains are shown in bold. The penetration depths are measured from the average phosphate plane to the C_α position for a given residue; a positive value indicates that the C_α atom is located below (deeper than) the phosphate plane. For a more extensive list of the residues, see Table S5 of the Supporting Information. [b]Averages over the final 400 ns of the trajectories of the first and second embedded models. [c]Averages over the final 100 ns of the trajectories of the first and second embedded models.

DOI: 10.1021/acs.biochem.5b00422
Biochemistry 2015, 54, 5696−5711

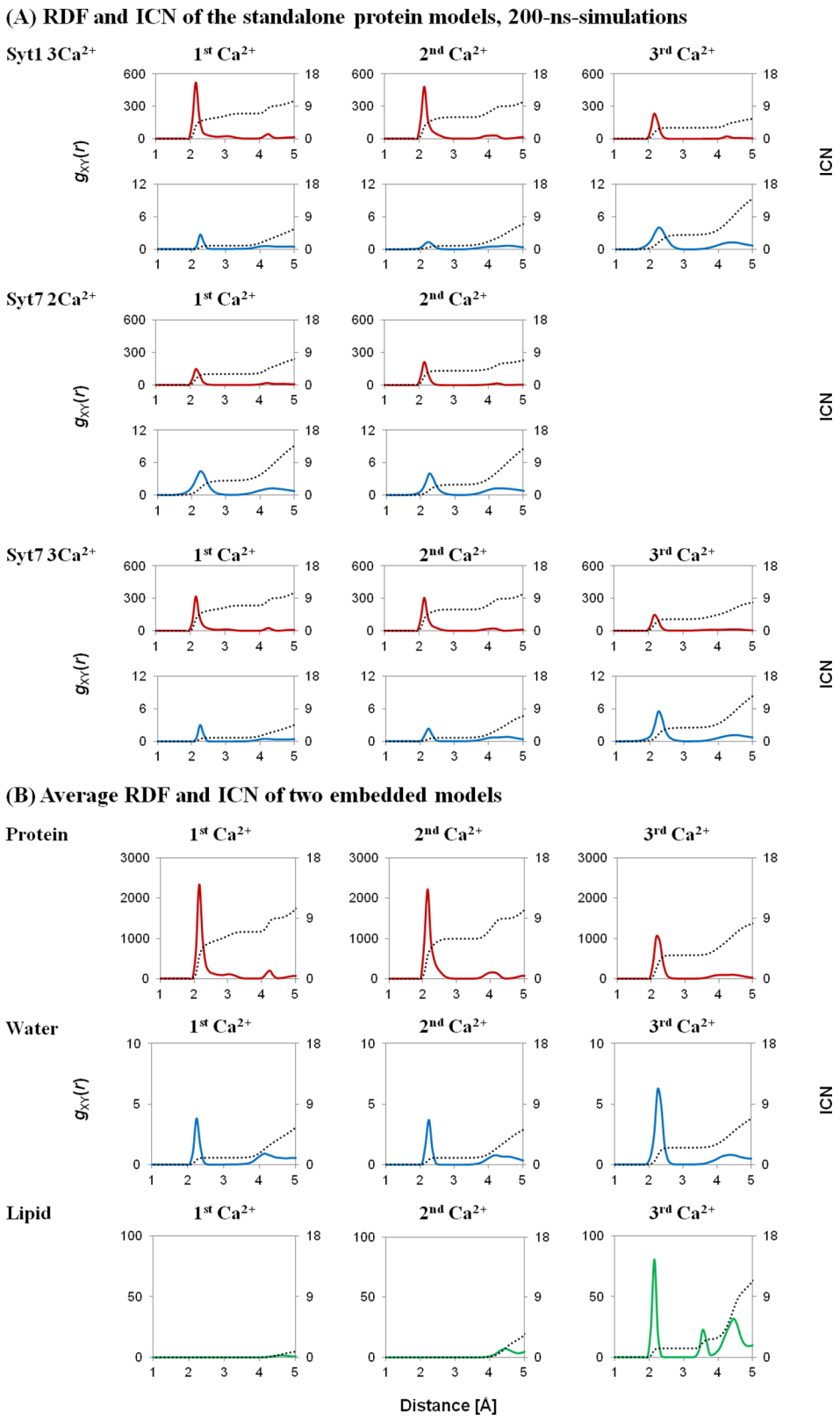

Figure 9. Radial distribution functions (RDFs) $g_{XY}(r)$ with corresponding integrated coordination numbers (ICN, dotted curves). (A) RDF and ICN from the stand-alone protein simulations. X = Ca^{2+}, and Y = oxygen of protein (red, top panel) or of water (blue, bottom panel). Averaged over the last 80 ns of each 200 ns simulation. (B) RDF and ICN from the embedded models. X = Ca^{2+}, and Y = oxygen of protein (red, top panel), of water (blue, middle panel), or of lipid (green, bottom panel). Averaged over the last 400 ns of both embedded simulations.

trajectories revealed that the flexible side chain of K184 was oriented toward the membrane in the starting structure used for the first simulation but away from the membrane in the second model (Figure S2). The residues in the CBLs that stayed near the phosphate plane (F167, S168, R228, S230, and R231) had >15 contacts with the lipid headgroups. F229 had the greatest

DOI: 10.1021/acs.biochem.5b00422
Biochemistry 2015, 54, 5696−5711

hydrophobic interaction with the lipid tails (45 contacts), and this residue also penetrated deepest (2.6 Å) into the membrane. F167 had the second-largest number of acyl chain contacts, even though its average penetration depth was above the membrane plane. However, the large standard deviation (2.9 Å) of its penetration depth reflects its frequent travel into and out of the acyl chain region during the simulations because of the seesaw-like movement of the C2A domain described above. By contrast, while R228, S230, and R231 had penetration depths similar to or greater than that of F167, they do not interact favorably with the hydrophobic tails and thus had small numbers of contacts with the acyl chain carbons.

For a closer look at how the F167 and F229 side chains interact with the fatty acyl tails of POPC and POPS, we have quantified the lipid contacts of these two phenyl rings as a function of the carbon number of the palmitoyl and oleoyl lipid chains (Figure S8). As expected, the contact numbers for F167 decrease monotonically from C2 to the lipid methyl ends, reflecting its dominant position near the phosphate plane. Interactions of F229 with C3−C5 were also substantial, consistent with its deeper penetration. Interestingly, while F167 and F229 had similar contacts with palmitoyl chain carbons, F229 had approximately twice the number of contacts as F167 with oleoyl chains. We suspect that the bent oleoyl chain is better able to accommodate the bulky insertion of CBL3, similar to a previous description of another deeply inserted C2 domain.[42]

Ca^{2+} Coordination in Stand-alone and Membrane-Bound Syt7 C2A. The binding of Ca^{2+} ions is critical to association of Syt7 C2A with membranes. As described above, our simulations of individual proteins support a stoichiometry of three bound Ca^{2+} ions for both Syt7 and Syt1 C2A, in agreement with measurements by Maximov et al.[15] To further illustrate the roles that the Ca^{2+} ions play in lipid coordination, we plot the radial distribution function (RDF) and the integrated coordination number (ICN) in Figure 9A for the stand-alone Syt7 C2A with three Ca^{2+} ions and in Figure 9B for the embedded protein−membrane complexes. RDF describes how the density of a particular coordinating atom (here, oxygen) varies as a function of the distance from the central atom or ion (here, Ca^{2+}), and ICN counts the total number of these coordinating atoms as a function of the distance from the center. Together, the RDF and ICN provide critical information about the coordination structures of the Ca^{2+} ions. For comparison, the RDF and ICN for the simulations of Syt1 C2A and the two-Ca^{2+} Syt7 C2A are given in Figure 9A, as well; the corresponding RDF and ICN for the preinsertion lying-down simulation are shown in Figure S9.

In the stand-alone simulations of Syt1 and Syt7 C2A with three Ca^{2+} ions, the first solvation shells of the Ca^{2+} ions were all located near r = 2.2 Å with a relatively narrow distribution of ~0.2 Å, where r is the distance between a Ca^{2+} ion and the surrounding O atoms. The total coordination numbers were 8 for the first Ca^{2+} ion and 7 for the second and third Ca^{2+} ions (Table 6), in agreement with previous experimental and computational studies that show coordination numbers of 6−8 depending on the salt concentration.[43−48] In both three-Ca^{2+} stand-alone models, the first and second Ca^{2+} ions were mostly solvated by the negatively charged side chains and the polar backbone carbonyl groups of the flexible CBL1−CBL3, with only one water coordinated to each Ca^{2+}. The third Ca^{2+} ion, which was water-free in the starting geometries (Figure 2B−D), became heavily solvated by four water molecules after equilibration. For comparison, the stand-alone two-Ca^{2+} Syt7 C2A had prominent contributions of water molecules to the solvation shells of both ions, with approximately half of the coordinating O atoms coming from water. The variations in the participation of water in the first and second Ca^{2+} coordination shells suggest that the binding of the third Ca^{2+} modifies the solvent coordination of the first two Ca^{2+} ions.

Table 6. Coordination Numbers of the First Solvation Shell for the Ca^{2+} Ions in the Binding Region of Syt7 C2A for the Stand-alone Protein and Protein−Membrane Complexes[a]

	first Ca^{2+}	second Ca^{2+}	third Ca^{2+}
Syt7 3-Ca^{2+} stand-alone			
protein oxygen	6.9	6.0	3.3
water oxygen	1.0	1.0	3.8
sum	7.9	7.0	7.1
embedded complexes			
protein oxygen	6.9	6.0	3.5
lipid oxygen	0	0	1.3
water oxygen	1.0	1.0	2.5
sum	7.9	7.0	7.3

[a]Taken to be the integrated coordination number at 3.25 Å. Values are averages over the final 80 ns of the simulations for the stand-alone protein and the final 400 ns of the simulations for the embedded complexes. Table S6 provides a more extensive list.

Compared with the membrane-free Syt7 C2A, the membrane-embedded Syt7 C2A has lipid headgroup O atoms in the coordination shell of the third Ca^{2+} ion (coordination number of 1.3), but no change for the first or second Ca^{2+} ion (Table 6 and Figure 9B). For the third Ca^{2+}, the lipid O atoms replaced water molecules, whereas the contributions of protein O atoms were largely identical between the two simulation conditions. The variations in the components of the solvation shell clearly indicate that the third Ca^{2+} ion not only helps to create a more favorable electrostatic environment for membrane association but also directly participates in C2A−lipid binding. Although the results presented here are obtained for Syt7 C2A, we suspect that the interaction between the outermost Ca^{2+} and membrane lipid may also exist in Syt1 C2A and other C2 domains and may contribute to the reported cooperativity in Ca^{2+} and membrane binding by many C2 domains.[49−51] For example, such an interaction would be consistent with the observation of Nalefski et al. that Ca^{2+} dissociates more rapidly from a membrane-free C2 domain than from a deeply membrane-inserted C2 domain.[49]

DISCUSSION

Summary of the Main Findings. Our simulations of binding of Syt7 C2A to Ca^{2+} and membranes support and extend the experimental measurements of its docking geometry reported in the preceding paper (DOI: 10.1021/acs.biochem.5b00421). The four most significant findings of the present study are as follows. (i) Syt7 C2A likely binds three Ca^{2+} ions, in agreement with NMR measurements,[15] and the third Ca^{2+} is coordinated by a combination of protein residues and water and/or lipid. (ii) When bound to Ca^{2+} ions and oriented with loops CBL1−CBL3 facing an anionic membrane, Syt7 C2A spontaneously approaches and inserts into the membrane. (iii) Three of four simulated geometries of the protein−membrane complex (all but the lying-down model) are qualitatively consistent with the orientation derived from EPR depth parameter measurements, even though the

DOI: 10.1021/acs.biochem.5b00422
Biochemistry 2015, 54, 5696−5711

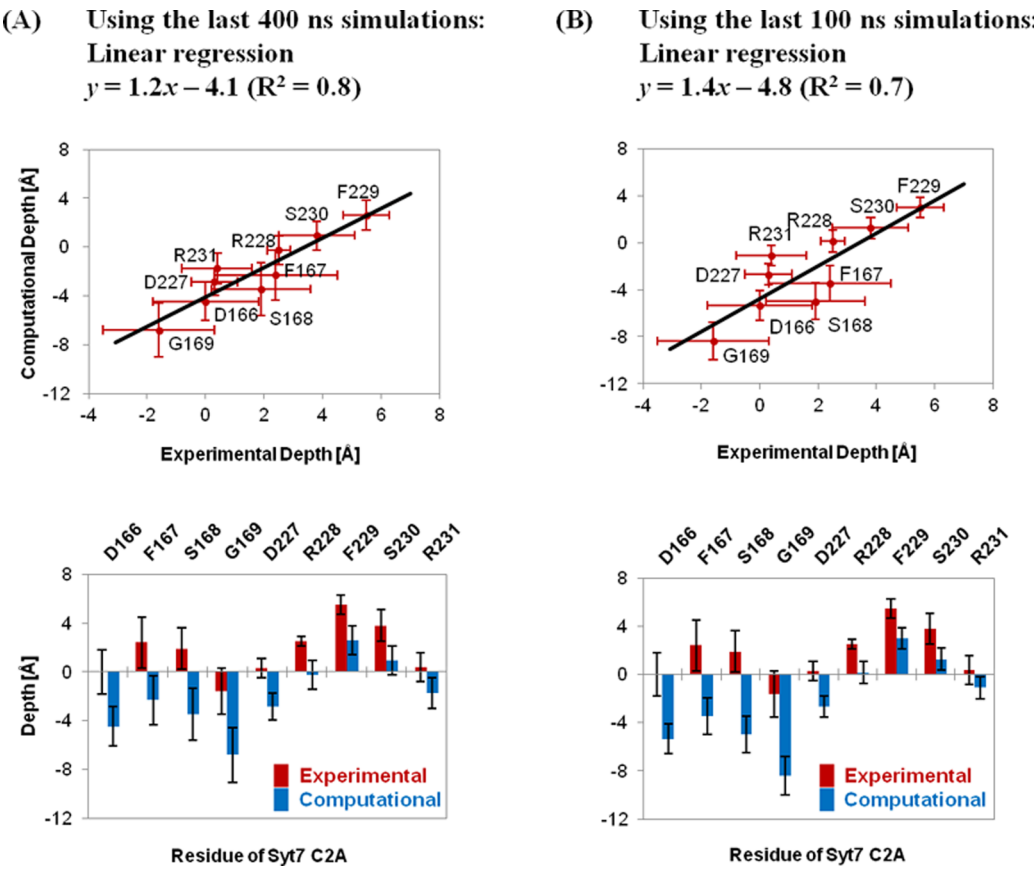

Figure 10. Comparison between experimental and computational membrane penetration depths of selected residues. The computational depths of α-carbons were averaged over (A) the last 400 ns and (B) the last 100 ns trajectories of both the first and second embedded models. Horizontal error bars indicate experimental statistical errors, and vertical error bars indicate computational statistical standard deviations. Bottom panels show side-by-side comparisons of penetration depths for each residue (red, experimental; blue, computational).

simulations were performed naïve of our EPR results. (iv) CBL1 appears to insert and retract dynamically in short simulations, suggesting low energy barriers for its initial insertion.

Overall, our results are consistent with a membrane docking mechanism triggered by an electrostatic switch of Ca^{2+} binding and stabilized by hydrophobic interactions between the membrane and the protein, primarily through CBL3 and secondarily through CBL1. Such a complex binding scenario of C2A domains mirrors the amphipathic nature of the phospholipid bilayer, as described earlier by Gerber et al.[52]

Comparison of Simulation and Experiment: Penetration Depths of Critical Residues in CBL1 and CBL3. The membrane docking geometry of a peripheral protein is described by (1) its angular orientation with respect to the membrane and (2) its depth of membrane penetration. Figure 10 shows a comparison of penetration depths for critical residues of Syt7 C2A between the simulations of the embedded protein–membrane complexes and the EPR experiments presented in the preceding paper (DOI: 10.1021/acs.biochem.5b00421) (see also Table S7 of the Supporting Information). Generally, the orientation of the protein domain agrees well with the experimental models as shown by the linear correlation between the experimental and simulated depths; however, the simulated depths are overall shallower in the simulations by ~4 Å (Figure 10). We emphasize that the experimental and computational determinations of the depths were conducted in parallel: the EPR docking geometry models used only the NMR protein structures[16] and the aqueous protein structures from our stand-alone protein MD simulations (section 3.2 of the Supporting Information), without input from our simulations of the protein–membrane complex. Conversely, the simulations of the protein–membrane complex were based on the available Syt7 C2A NMR structure and approximations to the published docking geometry of Syt1, rather than the EPR docking geometry reported in the preceding paper (DOI: 10.1021/acs.biochem.5b00421). This approach differs from some prior simulations of C2 domain membrane docking, which have started from the EPR-derived docking geometry.[53,54] From this point of view, the comparison presented here is a verification of predictions rather than a verification of fitting.

Depth differences between the EPR models and the simulations could arise, in principle, from several sources. The EPR-measured depths are associated with relatively large uncertainly, because of the dependence on the protein structure model and parameters chosen for the fitting procedure; however, the measurements clearly show higher depth parameters for residues in Syt7 C2A compared to equivalent positions in Syt1 C2A. In the simulations, systematic error could arise if the trajectories are not accurate representations of the highly dynamic and complex system; nevertheless, we observe that depths are stable and consistent among three trajectories (standing-up and two embedded) after simulation for 200–300 ns. Indeed, this observation seems to indicate that the standing-up simulation completed the insertion process

DOI: 10.1021/acs.biochem.5b00422
Biochemistry 2015, 54, 5696–5711

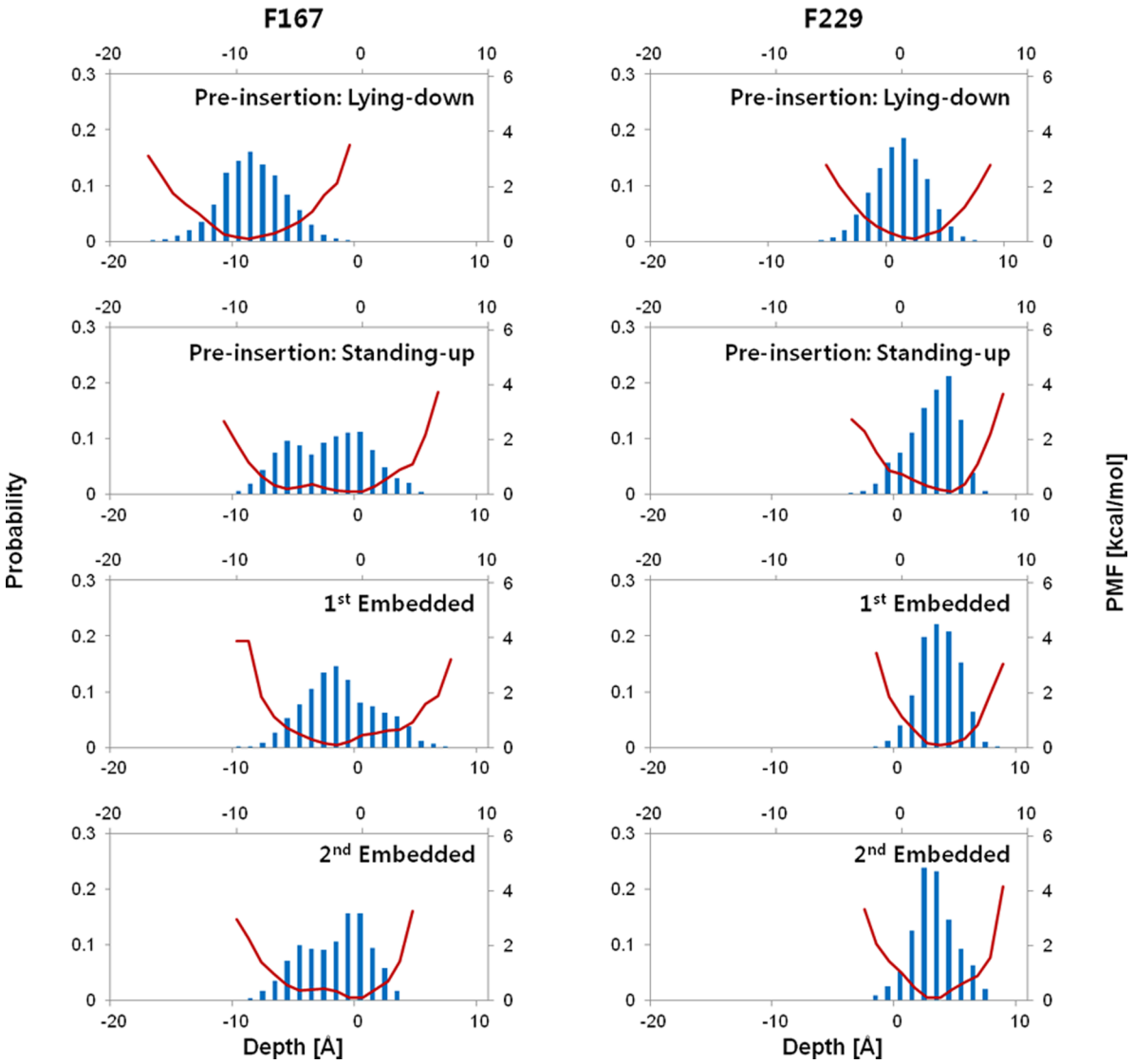

Figure 11. Probability distribution histograms (blue) and potential of mean force (PMF) curves (red) for the penetration depths of F167 and F229 from the indicated simulations of Syt7 C2A–membrane complexes. The results are based on the last 400 ns of each simulation.

after 300 ns, although this seems unexpectedly rapid for full insertion of this slow-acting Syt isoform. Rather, it is possible that the C2A domain did not fully reach equilibrium with respect to its penetration depth in the standing-up and two embedded model simulations. We have previously hypothesized a two-step model for Syt7 C2A membrane docking, including initial binding at a depth similar to that of Syt1 C2A and subsequent deeper penetration on an unknown time scale.[55] It is possible that the simulated model systems are trapped in a local minimum that corresponds to such an initial insertion state, while full insertion takes microseconds or longer. This would provide a possible explanation for the differences between the simulated depths and the EPR data, which were acquired on a time scale of minutes (Figure 10).

Substantially deeper embedding of the Syt7 C2A domain than in our present simulations would, however, present an interesting problem: it would require the first solvation shell of the third Ca^{2+} ion to be either partially or completely embedded in the membrane, which would involve losing its contacts with lipid headgroup oxygen atoms. Presumably, such a penetration would have to involve a structural rearrangement of either protein or lipids to maintain coordination of the third Ca^{2+} ion. The 500 ns simulations presented here do not suggest significant conformational changes of C2A, as evident from the similar rmsd values of the protein backbone between the membrane-free and membrane-bound C2A (Figure S4 of the Supporting Information). The minor decrease in average rmsd (Table 2) from 1.8 Å in the protein alone (bound to three Ca^{2+} ions) to 1.5 Å in the simulations of preinsertion models to 1.2 Å in the embedded simulations is likely due to the increased number of restraints from interactions with the membrane. Of course, we cannot rule out substantial larger changes in the C2A or lipid conformation over longer time scales. In principle, it is also possible that the third Ca^{2+} is shed during the penetration process along with a structural rearrangement of protein and/or lipid. We are not aware of any explicit experimental measurement of Ca^{2+} stoichiometry for membrane-bound Syt7 C2A. However, we note that a recent computational study on Syt1 C2AB suggested that the C2A domain may stably bind only two Ca^{2+} ions.[56] Further studies are needed to resolve whether structural rearrangements may

DOI: 10.1021/acs.biochem.5b00422
Biochemistry 2015, 54, 5696–5711

accommodate or remove the third Ca^{2+} to facilitate deeper membrane penetration for Syt7 C2A.

Dynamics of CBL1 and Forces Favoring Different Modes of Docking. Our simulations suggest that the Syt7 C2A domain docks to the membrane in a dynamic manner, in that the protein orientation fluctuates considerably over time with respect to the membrane. The average tilt angle is a simplified characterization for this dynamic insertion. Figure S10 displays the histogram of the tilt angles for all protein−membrane complexes as well as the associated potential of mean force (PMF) curves, which were computed through Boltzmann inversion on the basis of the probability distributions. The PMF curves for the embedded and standing-up models each exhibit a flat-bottom well >30° in width and roughly centered at 35°. The preinsertion lying-down model featured a narrower well (spanning ∼20°), whose center was at a smaller angle of 15°. As discussed earlier, the broad wells suggest a competition between the electrostatic attraction of the positively charged residues by the lipid headgroups and the stabilization of F167 by the hydrophobic lipid tails. The lying-down position favors the former interaction, giving rise to the smaller tilt angle and narrower distribution. Even so, at 298 K, the protein in the lying-down simulation still had substantial probability of sampling a large tilt angle.

The penetration depths of F167 and F229 also illustrate the dynamic nature of the docked state. Figure 11 shows histograms of the depths of their C_α atoms and the associated PMF profiles. Qualitatively, the plots indicate that the simulation of the preinsertion lying-down model differs from the other three simulations (standing-up and two embedded); in the latter, F167 could almost freely enter and leave the membrane while F229 was stabilized 4 Å below the phosphate plane. It should be kept in mind that PMF curves are most reliable at the bottom of the well because of poor sampling in regions far from the minimum. Nevertheless, qualitatively, the plots clearly indicate that F229 is critical in anchoring the C2A domain to the membrane. This finding echoes the strict conservation of this residue among mammalian Syt C2A domains. By contrast, the residue at the tip of CBL1 is Phe in Syt7, Met in Syt1, and variable among other isoforms (Figure S1).

Finally, we note that the competition between electrostatic attraction of the β4 strand with PS headgroups and the insertion of CBL1 can be resolved if the target membrane contains negative curvature. Although induction of curvature by Syt7 C2A has not been reported, Syt1 C2B has been reported to curve membranes and negative Gaussian curvature is present in the exocytotic fusion pore.[57] Simultaneous stabilization of both electrostatic and hydrophobic interactions could possibly overcome free energy barriers associated with coordination of the third Ca^{2+} upon deeper insertion of Syt7 C2A. More broadly, further studies are needed to describe the relationship between membrane penetration and curvature for the synaptotagmin family as a whole.

■ ASSOCIATED CONTENT

Supporting Information

The Supporting Information is available free of charge on the ACS Publications website at DOI: 10.1021/acs.biochem.5b00422.

Supplementary details of model construction, MD simulations, and data analysis; dimensions and numbers of atoms for models (Table S1); initial harmonic restraints in energy minimizations for building protein−membrane complexes (Tables S2 and S3); statistics of the tilt angle and the penetration depths of F167 and F229 for the protein−membrane complexes (Table S4); the average number of contacts with lipid headgroups and acyl chains for each protein residue (Table S5); coordination numbers of the first solvation shell for the Ca^{2+} ions (Table S6); experimental versus computational depths of penetration for the loop residues (Table S7); sequence comparison of CBL regions among mammalian Syt isoforms (Figure S1); orientations of K184 in the two embedded models (Figure S2); area per lipid and lipid order parameters of the 3:1 POPC/POPS membrane (Figure S3); rmsd of protein backbone heavy atoms (Figure S4); electrostatic potential surfaces of Syt1 and Syt7 C2A domains (Figure S5); comparison of protein tilt angles with penetration depths of F167 and F229 (Figure S6); total number of heavy atom contacts between C2A and lipid headgroups for the embedded models (Figure S7); counts of lipid tail carbon atoms in the proximity of F167 and F229 (Figure S8); radial distribution functions for the preinsertion lying-down and standing-up simulations (Figure S9); probability distribution histogram and potential of mean force versus tilt angle for Syt7 C2A−membrane complexes (Figure S10); and tilt angles of the protein and penetration depths of the protein center of mass, F167, and F229 for the preinsertion standing-up model with NBFIX parameter-corrected Na^+ (Figure S11) and K^+ (Figure S12) (PDF)

■ AUTHOR INFORMATION

Corresponding Authors

*E-mail: jefferson.knight@ucdenver.edu.

*E-mail: hai.lin@ucdenver.edu.

Funding

This work is supported by Multi-Investigator Cottrell College Science Award 22399 from the Research Corporation for Science Advancement to J.D.K. and H.L. and by Grant CHE-140070 for use of the Extreme Science and Engineering Discovery Environment (XSEDE), which is supported by National Science Foundation Grant ACI-1053575. H.L. also thanks the Camille & Henry Dreyfus Foundation for support (TH-14-028). J.D.K. thanks the National Institutes of Health for support (R15GM102866). N.R. acknowledges support from the Research Council of Norway (grant FRIMEDBIO #214167) and computational time from the Norwegian metacenter for computational science (NOTUR).

Notes

The authors declare no competing financial interest.

■ ACKNOWLEDGMENTS

We thank Soroosh Pezeshki, Christal Davis, and Prof. Emad Tajkhorshid for helpful discussions.

■ ABBREVIATIONS

Syt1, synaptotagmin 1; Syt7, synaptotagmin 7; CBL, Ca^{2+} binding loop; POPC, 1-palmitoyl-2-oleoyl-*sn*-glycero-3-phosphocholine; POPS, 1-palmitoyl-2-oleoyl-*sn*-glycero-3-phospho-

DOI: 10.1021/acs.biochem.5b00422
Biochemistry 2015, 54, 5696−5711

L-serine; EPR, electron paramagnetic resonance; CHARMM, chemistry at Harvard macromolecular mechanics; VMD, visual molecular dynamics; NAMD, nanoscale molecular dynamics; MD, molecular dynamics; APL, area per lipid; RDF, radial distribution function; PMF, potential of mean force.

REFERENCES

(1) Chapman, E. R. (2008) How does synaptotagmin trigger neurotransmitter release? *Annu. Rev. Biochem. 77*, 615−641.

(2) Gustavsson, N., and Han, W. (2009) Calcium-sensing beyond neurotransmitters: functions of synaptotagmins in neuroendocrine and endocrine secretion. *Biosci. Rep. 29*, 245−259.

(3) Gauthier, B. R., and Wollheim, C. B. (2008) Synaptotagmins bind calcium to release insulin. *Am. J. Physiol. Endocrinol. Metab 295*, E1279−1286.

(4) Sudhof, T. C., and Rothman, J. E. (2009) Membrane fusion: grappling with SNARE and SM proteins. *Science 323*, 474−477.

(5) Nalefski, E. A., and Falke, J. J. (1996) The C2 domain calcium-binding motif: structural and functional diversity. *Protein Sci. 5*, 2375−2390.

(6) Egea-Jimenez, A. L., Fernandez-Martinez, A. M., Perez-Lara, A., de Godos, A., Corbalan-Garcia, S., and Gomez-Fernandez, J. C. (2014) Phosphatidylinositol-4,5-bisphosphate enhances anionic lipid demixing by the C2 domain of PKCα. *PLoS One 9*, e95973.

(7) Nalefski, E. A., Wisner, M. A., Chen, J. Z., Sprang, S. R., Fukuda, M., Mikoshiba, K., and Falke, J. J. (2001) C2 domains from different Ca^{2+} signaling pathways display functional and mechanistic diversity. *Biochemistry 40*, 3089−3100.

(8) Kohout, S. C., Corbalan-Garcia, S., Torrecillas, A., Gomez-Fernandez, J. C., and Falke, J. J. (2002) C2 domains of protein kinase C isoforms alpha, beta, and gamma: activation parameters and calcium stoichiometries of the membrane-bound state. *Biochemistry 41*, 11411−11424.

(9) Stahelin, R. V., Rafter, J. D., Das, S., and Cho, W. (2003) The molecular basis of differential subcellular localization of C2 domains of protein kinase Cα and group IVa cytosolic phospholipase A2. *J. Biol. Chem. 278*, 12452−12460.

(10) Brandt, D. S., Coffman, M. D., Falke, J. J., and Knight, J. D. (2012) Hydrophobic contributions to the membrane docking of Synaptotagmin 7 C2A domain: Mechanistic contrast between isoforms 1 and 7. *Biochemistry 51*, 7654−7664.

(11) Hui, E., Bai, J., Wang, P., Sugimori, M., Llinas, R. R., and Chapman, E. R. (2005) Three distinct kinetic groupings of the synaptotagmin family: candidate sensors for rapid and delayed exocytosis. *Proc. Natl. Acad. Sci. U. S. A. 102*, 5210−5214.

(12) Sugita, S., Shin, O. H., Han, W., Lao, Y., and Sudhof, T. C. (2002) Synaptotagmins form a hierarchy of exocytotic Ca^{2+} sensors with distinct Ca^{2+} affinities. *EMBO J. 21*, 270−280.

(13) Zhang, X., Rizo, J., and Sudhof, T. C. (1998) Mechanism of phospholipid binding by the C2A-domain of synaptotagmin I. *Biochemistry 37*, 12395−12403.

(14) Frazier, A. A., Roller, C. R., Havelka, J. J., Hinderliter, A., and Cafiso, D. S. (2003) Membrane-bound orientation and position of the Synaptotagmin I C2A domain by site-directed spin labeling. *Biochemistry 42*, 96−105.

(15) Maximov, A., Lao, Y., Li, H., Chen, X., Rizo, J., Sørensen, J. B., and Südhof, T. C. (2008) Genetic analysis of synaptotagmin-7 function in synaptic vesicle exocytosis. *Proc. Natl. Acad. Sci. U. S. A. 105*, 3986−3991.

(16) Nagashima, T., Hayashi, F., and Yokoyama, S. (2015) Solution structure of the first C2 domain of synaptotagmin VII, unpublished results.

(17) Jo, S., Kim, T., Iyer, V. G., and Im, W. (2008) CHARMM-GUI: A web-based graphical user interface for CHARMM. *J. Comput. Chem. 29*, 1859−1865.

(18) Klauda, J. B., Venable, R. M., Freites, J. A., O'Connor, J. W., Tobias, D. J., Mondragon-Ramirez, C., Vorobyov, I., MacKerell, A. D., and Pastor, R. W. (2010) Update of the CHARMM all-atom additive force field for lipids: Validation on six lipid types. *J. Phys. Chem. B 114*, 7830−7843.

(19) Jorgensen, W. L., Chandrasekhar, J., Madura, J. D., Impey, R. W., and Klein, M. L. (1983) Comparison of simple potential functions for simulating liquid water. *J. Chem. Phys. 79*, 926−935.

(20) Phillips, J. C., Braun, R., Wang, W., Gumbart, J., Tajkhorshid, E., Villa, E., Chipot, C., Skeel, R. D., Kale, L., and Schulten, K. (2005) Scalable molecular dynamics with NAMD. *J. Comput. Chem. 26*, 1781−1802.

(21) Brooks, B. R., Brooks, C. L., Mackerell, A. D., Nilsson, L., Petrella, R. J., Roux, B., Won, Y., Archontis, G., Bartels, C., Boresch, S., Caflisch, A., Caves, L., Cui, Q., Dinner, A. R., Feig, M., Fischer, S., Gao, J., Hodoscek, M., Im, W., Kuczera, K., Lazaridis, T., Ma, J., Ovchinnikov, V., Paci, E., Pastor, R. W., Post, C. B., Pu, J. Z., Schaefer, M., Tidor, B., Venable, R. M., Woodcock, H. L., Wu, X., Yang, W., York, D. M., and Karplus, M. (2009) CHARMM: The biomolecular simulation program. *J. Comput. Chem. 30*, 1545−1614.

(22) MacKerell, A. D., Jr., Bashford, D., Bellott, M., Dunbrack, R. L., Evanseck, J. D., Field, M. J., Fischer, S., Gao, J., Guo, H., Ha, S., Joseph-McCarthy, D., Kuchnir, L., Kuczera, K., Lau, F. T. K., Mattos, C., Michnick, S., Ngo, T., Nguyen, D. T., Prodhom, B., Reiher, W. E., III, Roux, B., Schlenkrich, M., Smith, J. C., Stote, R., Straub, J., Watanabe, M., Wiorkiewicz-Kuczera, J., Yin, D., and Karplus, M. (1998) All-atom empirical potential for molecular modeling and dynamics studies of proteins. *J. Phys. Chem. B 102*, 3586−3616.

(23) Mackerell, A. D., Feig, M., and Brooks, C. L. (2004) Extending the treatment of backbone energetics in protein force fields: Limitations of gas-phase quantum mechanics in reproducing protein conformational distributions in molecular dynamics simulations. *J. Comput. Chem. 25*, 1400−1415.

(24) Humphrey, W., Dalke, A., and Schulten, K. (1996) VMD: Visual molecular dynamics. *J. Mol. Graphics 14*, 33−38.

(25) Shao, X., Fernandez, I., Sudhof, T. C., and Rizo, J. (1998) Solution structures of the Ca^{2+}-free and Ca^{2+}-bound C2A domain of synaptotagmin I: Does Ca^{2+} induce a conformational change? *Biochemistry 37*, 16106−16115.

(26) Baker, N. A., Sept, D., Joseph, S., Holst, M. J., and McCammon, J. A. (2001) Electrostatics of nanosystems: Application to microtubules and the ribosome. *Proc. Natl. Acad. Sci. U. S. A. 98*, 10037−10041.

(27) Seelig, J., and Waespe-Sarcevic, N. (1978) Molecular order in cis and trans unsaturated phospholipid bilayers. *Biochemistry 17*, 3310−3315.

(28) Venable, R. M., Luo, Y., Gawrisch, K., Roux, B., and Pastor, R. W. (2013) Simulations of anionic lipid membranes: Development of interaction-specific ion parameters and validation using NMR data. *J. Phys. Chem. B 117*, 10183−10192.

(29) Sutton, R. B., Davletov, B. A., Berghuis, A. M., Sudhof, T. C., and Sprang, S. R. (1995) Structure of the first C2 domain of synaptotagmin I: A novel Ca^{2+}/phospholipid-binding fold. *Cell 80*, 929−938.

(30) Ubach, J., Zhang, X., Shao, X., Sudhof, T. C., and Rizo, J. (1998) Ca^{2+} binding to synaptotagmin: how many Ca^{2+} ions bind to the tip of a C2-domain? *EMBO J. 17*, 3921−3930.

(31) Vrljic, M., Strop, P., Ernst, J. A., Sutton, R. B., Chu, S., and Brunger, A. T. (2010) Molecular mechanism of the synaptotagmin-SNARE interaction in Ca^{2+}-triggered vesicle fusion. *Nat. Struct. Mol. Biol. 17*, 325−331.

(32) Bhalla, A., Chicka, M. C., and Chapman, E. R. (2008) Analysis of the synaptotagmin family during reconstituted membrane fusion. Uncovering a class of inhibitory isoforms. *J. Biol. Chem. 283*, 21799−21807.

(33) Murray, D., and Honig, B. (2002) Electrostatic control of the membrane targeting of C2 domains. *Mol. Cell 9*, 145−154.

(34) Herrick, D. Z., Sterbling, S., Rasch, K. A., Hinderliter, A., and Cafiso, D. S. (2006) Position of synaptotagmin I at the membrane interface: cooperative interactions of tandem C2 domains. *Biochemistry 45*, 9668−9674.

DOI: 10.1021/acs.biochem.5b00422
Biochemistry 2015, 54, 5696−5711

(35) Vennekate, W., Schroder, S., Lin, C. C., van den Bogaart, G., Grunwald, M., Jahn, R., and Walla, P. J. (2012) Cis- and trans-membrane interactions of synaptotagmin-1. *Proc. Natl. Acad. Sci. U. S. A. 109*, 11037−11042.
(36) Vasquez, J. K., Chantranuvatana, K., Giardina, D. T., Coffman, M. D., and Knight, J. D. (2014) Lateral diffusion of proteins on supported lipid bilayers: Additive friction of synaptotagmin 7 C2A-C2B tandem domains. *Biochemistry 53*, 7904−7913.
(37) Herrick, D. Z., Kuo, W., Huang, H., Schwieters, C. D., Ellena, J. F., and Cafiso, D. S. (2009) Solution and membrane-bound conformations of the tandem C2A and C2B domains of synaptotagmin 1: Evidence for bilayer bridging. *J. Mol. Biol. 390*, 913−923.
(38) Hui, E., Bai, J., and Chapman, E. R. (2006) Ca^{2+}-triggered simultaneous membrane penetration of the tandem C2-domains of synaptotagmin I. *Biophys. J. 91*, 1767−1777.
(39) Frazier, A. A., Wisner, M. A., Malmberg, N. J., Victor, K. G., Fanucci, G. E., Nalefski, E. A., Falke, J. J., and Cafiso, D. S. (2002) Membrane orientation and position of the C2 domain from cPLA2 by site-directed spin labeling. *Biochemistry 41*, 6282−6292.
(40) Landgraf, K. E., Malmberg, N. J., and Falke, J. J. (2008) Effect of PIP2 binding on the membrane docking geometry of PKCα C2 domain: An EPR site-directed spin-labeling and relaxation study. *Biochemistry 47*, 8301−8316.
(41) Lai, C.-L., Landgraf, K. E., Voth, G. A., and Falke, J. J. (2010) Membrane docking geometry and target lipid stoichiometry of membrane-bound PKCα C2 domain: A combined molecular dynamics and experimental study. *J. Mol. Biol. 402*, 301−310.
(42) Jaud, S., Tobias, D. J., Falke, J. J., and White, S. H. (2007) Self-induced docking site of a deeply embedded peripheral membrane protein. *Biophys. J. 92*, 517−524.
(43) Tongraar, A., Liedl, K. R., and Rode, B. M. (1997) Solvation of Ca^{2+} in water studied by Born-Oppenheimer ab initio QM/MM dynamics. *J. Phys. Chem. A 101*, 6299−6309.
(44) Jalilehvand, F., Spångberg, D., Lindqvist-Reis, P., Hermansson, K., Persson, I., and Sandström, M. (2001) Hydration of the calcium ion. An EXAFS, large-angle X-ray scattering, and molecular dynamics simulation study. *J. Am. Chem. Soc. 123*, 431−441.
(45) Naor, M. M., Nostrand, K. V., and Dellago, C. (2003) Car−Parrinello molecular dynamics simulation of the calcium ion in liquid water. *Chem. Phys. Lett. 369*, 159−164.
(46) Remko, M., and Rode, B. M. (2006) Effect of metal ions (Li^+, Na^+, K^+, Mg^{2+}, Ca^{2+}, Ni^{2+}, Cu^{2+}, and Zn^{2+}) and water coordination on the structure of glycine and zwitterionic glycine. *J. Phys. Chem. A 110*, 1960−1967.
(47) Cappa, C. D., Smith, J. D., Messer, B. M., Cohen, R. C., and Saykally, R. J. (2006) Effects of cations on the hydrogen bond network of liquid water: New results from X-ray absorption spectroscopy of liquid microjets. *J. Phys. Chem. B 110*, 5301−5309.
(48) Pirc, E. T., Zidar, J., and Bukovec, P. (2012) A computational study of calcium(II) and copper(II) ion binding to the hyaluronate molecule. *Int. J. Mol. Sci. 13*, 12036−12045.
(49) Nalefski, E. A., Slazas, M. M., and Falke, J. J. (1997) Ca^{2+}-signaling cycle of a membrane-docking C2 domain. *Biochemistry 36*, 12011−12018.
(50) Radhakrishnan, A., Stein, A., Jahn, R., and Fasshauer, D. (2009) The Ca^{2+} affinity of synaptotagmin 1 is markedly increased by a specific interaction of its C2B domain with phosphatidylinositol 4,5-bisphosphate. *J. Biol. Chem. 284*, 25749−25760.
(51) Corbin, J. A., Evans, J. H., Landgraf, K. E., and Falke, J. J. (2007) Mechanism of specific membrane targeting by C2 domains: Localized pools of target lipids enhance Ca^{2+} affinity. *Biochemistry 46*, 4322−4336.
(52) Gerber, S. H., Rizo, J., and Südhof, T. C. (2002) Role of electrostatic and hydrophobic interactions in Ca^{2+}-dependent phospholipid binding by the C2A-domain from synaptotagmin I. *Diabetes 51*, S12−S18.
(53) Jaud, S., Tobias, D. J., Falke, J. J., and White, S. H. (2007) Self-induced docking site of a deeply embedded peripheral membrane protein. *Biophys. J. 92*, 517−524.
(54) Lai, C. L., Landgraf, K. E., Voth, G. A., and Falke, J. J. (2010) Membrane docking geometry and target lipid stoichiometry of membrane-bound PKCalpha C2 domain: a combined molecular dynamics and experimental study. *J. Mol. Biol. 402*, 301−310.
(55) Brandt, D. S., Coffman, M. D., Falke, J. J., and Knight, J. D. (2012) Hydrophobic contributions to the membrane docking of synaptotagmin 7 C2A domain: mechanistic contrast between isoforms 1 and 7. *Biochemistry 51*, 7654−7664.
(56) Bykhovskaia, M. (2015) Calcium binding promotes conformational flexibility of the neuronal Ca^{2+} sensor synaptotagmin. *Biophys. J. 108*, 2507−2520.
(57) Hui, E., Johnson, C. P., Yao, J., Dunning, F. M., and Chapman, E. R. (2009) Synaptotagmin-mediated bending of the target membrane is a critical step in Ca^{2+}-regulated fusion. *Cell 138*, 709−721.
(58) Kučerka, N., Nieh, M.-P., and Katsaras, J. (2011) Fluid phase lipid areas and bilayer thicknesses of commonly used phosphatidylcholines as a function of temperature. *Biochim. Biophys. Acta, Biomembr. 1808*, 2761−2771.
(59) Böckmann, R. A., Hac, A., Heimburg, T., and Grubmüller, H. (2003) Effect of sodium chloride on a lipid bilayer. *Biophys. J. 85*, 1647−1655.
(60) Mukhopadhyay, P., Monticelli, L., and Tieleman, D. P. (2004) Molecular dynamics simulation of a palmitoyl-oleoyl phosphatidylserine bilayer with Na^+ counterions and NaCl. *Biophys. J. 86*, 1601−1609.

DOI: 10.1021/acs.biochem.5b00422
Biochemistry 2015, 54, 5696−5711